Three-Dimensional Analytical Field Calculation of Pyramidal-Frustum Shaped Permanent Magnets

J. L. G. Janssen, J. J. H. Paulides, and E. A. Lomonova

Department of Electrical Engineering, Group of Electromechanics and Power Electronics, Eindhoven University of Technology, 5612 AZ Eindhoven, The Netherlands

This paper presents a novel method to obtain fully analytical expressions of the magnetic field created by a pyramidal-frustum shaped permanent magnet. Conventional analytical tools only provide expressions for cuboidal permanent magnets and this paper extends these tools to more complex shapes. A novel analytical model for the magnetic field induced by triangular charged surfaces is combined with the field expressions for rectangular charged surfaces. This provides a fully analytical expression for the magnetic field of a pyramidal-frustum shaped permanent magnet. Field and force obtained using this model are validated with Finite Element Modeling.

***Index Terms*—Actuators, magnetic levitation, magnets, modeling, permanent magnets, permanent magnet machines, vibrations.**

I. Introduction

PERMANENT MAGNET (PM)-based gravity compensation is a relatively new but increasingly used technique in vibration isolation devices [1]–[3]. Conventional techniques, such as hydraulic or air-based gravity compensators, generally exhibit higher force density and are technically more mature compared to PM based devices. However, PM based vibration isolation provides a high control bandwidth and reduced energy consumption with respect to the previously mentioned techniques, and is for this reason considered a feasible alternative for the conventional techniques.

In order to achieve high positioning requirements and simultaneously minimized energy consumption it is essential that the PM modeling accuracy is maximized. In this way the effort required from the controller and with this the energy consumption is minimized, since the controller does not need to compensate for large modeling errors. Another demand for the machine model is a low calculation time, which enables quick and efficient topology optimization.

It is shown in [3] that the PM topology of a gravity compensator is of significant influence on the produced force. More specifically, topologies which focus the magnetic flux to a small volume, such as the Halbach topology, provide the highest force density. In [3], solely cuboidal PMs are used to investigate the achievable force density for bidirectional (or checkerboard) arrays and Halbach arrays. Increased flux focusing properties, hence, increased force density, may be achieved by means of differently shaped PMs, such as the 3D trapezoidal magnets in this paper.

Models with trapezoidal permanent magnets have been implemented for translating and for spherical electrical machines in [4]–[6]. In many cases, harmonic field modeling is a very suitable method, as a result of the inherent geometrical periodicity of the topology and negligible end effects. However, in a high-precision gravity compensator the end effects should be incorporated, since this increases the model accuracy. Additionally, the field at the edges of the device can be used as part of active devices which provide stability and accuracy.

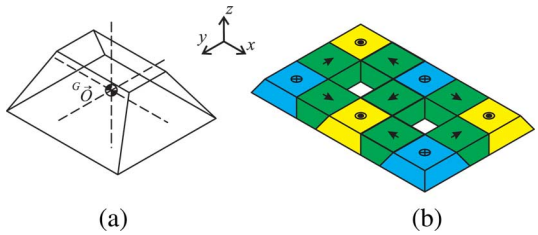

Fig. 1. (a) Pyramidal frustum and (b) Halbach array with pyramidal frusta.

Therefore, analytical charge modeling [7], [8] is used in this paper, since it provides exact, non-discrete field modeling of the PM. The 2D trapezoidal PMs in the Halbach topology described in [4]–[6], become 3D pyramidal frustums in the 3D cartesian coordinate system, as shown in Fig. 1(a). An example of the resulting Halbach array is shown in Fig. 1(b).

The variables which define the pyramidal frustum are explained in Section II. Section III then elaborates on the separation of the side surfaces into more simple geometrical shapes, for which the field expressions are derived. The resulting field expressions are validated in Section IV. Finally, Section V presents conclusions on the feasibility of the analytical expressions.

II. Definitions of the Pyramidal Frustum

The pyramidal frustum, or 3D trapezoidal PM, is defined in Fig. 2. The dimensions of the top surface are defined by a_{top} and b_{top}, and those for the bottom surface by a_{bot} and b_{bot}, respectively. By reducing a_{top} and b_{top} towards zero, a pyramidal shape is obtained. The angles $\alpha_{1\ldots4}$ are defined counterclockwise, hence α_1 and α_4 are positive, and α_2 and α_3 are negative. The rectangular bottom and top surfaces are parallel but do not necessarily share the same symmetry axis, hence α_1 and α_3 are not automatically equal. The same is valid for α_2 and α_4.

The origin of the reference coordinate system, $^G\vec{O}$, is at the center of mass of the pyramidal frustum. The prefix G indicates that the vector $\vec{O}$ is expressed in global coordinates. Each side

Manuscript received March 06, 2009; revised April 04, 2009. Current version published September 18, 2009. Corresponding author: J. L. G. Janssen (e-mail: j.l.g.janssen@tue.nl).

Color versions of one or more of the figures in this paper are available online at http://ieeexplore.ieee.org.

Digital Object Identifier 10.1109/TMAG.2009.2021861

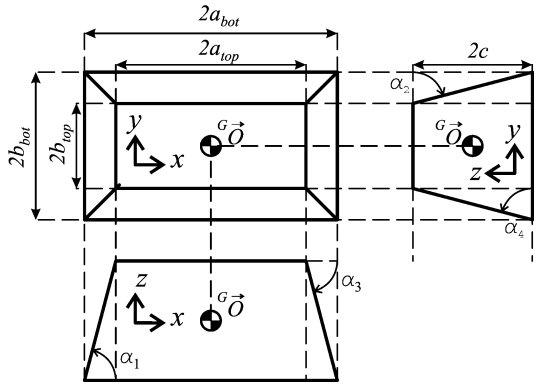

Fig. 2. Definition of the variables in the pyramidal frustum.

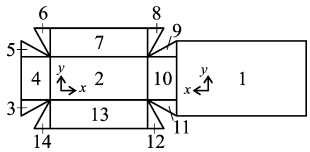

Fig. 3. Unfolded pyramidal frustum with fourteen segments.

surface of the pyramidal frustum has its own local coordinate system, hereafter referred to with the prefix L. In Section III.C these prefixes are used extensively to distinguish the various coordinate systems.

III. Field Calculation

The novel analytical expression for the magnetic field of the pyramidal-frustum shaped PM is derived by identifying fourteen individual geometrical surfaces. Each trapezoidal side plane is cut into one rectangular and two triangular planes, as is shown in the unfolded pyramidal frustum of Fig. 3. For each surface, the analytical field is obtained individually. Two surface types, rectangular and triangular, are now distinguished.

A. Field of the Rectangular Charged Surface

The field expressions for the rectangular charged surface apply to surfaces 1, 2, 4, 7, 10 and 13. These analytical expressions are found in [7].

B. Field of the Triangular Charged Surface

The field expressions for the triangular charged surface apply to surfaces 3, 5, 6, 8, 9, 11, 12 and 14. Fig. 4 shows that two orientations, $\triangle 1$ and $\triangle 2$, of the triangular surface are distinguished. Each of these surfaces is the result of a 180° rotation of the other around the y-axis and therefore both charged surfaces have slightly different field expressions. Fig. 4 also shows the location of the origin, $\vec{O}_{\triangle}$.

The complete expressions for the triangular charged surfaces are proposed in [9]. In this paper, only a basic derivation is presented. The general expression for the magnetic field of a uniformly magnetized permanent magnet in free space is [10]

$$\vec{B}(\vec{r}) = \frac{\mu_0}{4\pi} \oint_S \frac{\sigma(\vec{r}-\vec{r}')}{|\vec{r}-\vec{r}'|^3} \mathrm{d}s'. \tag{1}$$

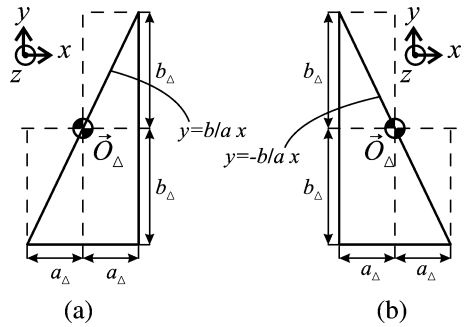

Fig. 4. Definition of the variables in triangular surfaces (a) $\triangle 1$ and (b) $\triangle 2$.

TABLE I
Definitions of the Integrands and Integration Limits for the Inner and Outer Integrals of (2)

Triangular surf.	Axis	Inner integral	Outer integral
$\triangle 1$	x	$\frac{a_\triangle}{b_\triangle} y' \le x' \le a_\triangle$	$-b_\triangle \le y' \le b_\triangle$
$\triangle 1$	y, z	$-b_\triangle \le y' \le \frac{b_\triangle}{a_\triangle} x'$	$-a_\triangle \le x' \le a_\triangle$
$\triangle 2$	x	$-a_\triangle \le x' \le -\frac{a_\triangle}{b_\triangle} y'$	$-b_\triangle \le y' \le b_\triangle$
$\triangle 2$	y, z	$-b_\triangle \le y' \le -\frac{b_\triangle}{a_\triangle} x'$	$-a_\triangle \le x' \le a_\triangle$

In this equation σ represents the magnetic charge density, and $\vec{r}$ is a position vector defined by $[x\ y\ z]^T$. The integration surface is S, which is triangular (Fig. 4). The resulting x-component of the magnetic flux density of surface $\triangle 1$ is now given by

$$B_{\triangle 1_x}(\vec{r}) = \frac{\mu_0 \sigma}{4\pi} \int_{-b}^{b} \left[\int_{\frac{a}{b}y'}^{a} \frac{x-x'}{|\vec{r}-\vec{r}'|^3} \mathrm{d}x' \right] \mathrm{d}y'. \tag{2}$$

Similarly, the integration limits of the other field components are derived. Table I shows for each field component which variable is in the inner and which is in the outer integral, and it shows what the respective integration limits are. As mentioned at the beginning of this Section, exact solutions are presented in [9].

The field expressions of surfaces $\triangle 1$ and $\triangle 2$ complement each other, or

$$\vec{B}_{\triangle 1}(\vec{r}) = \boldsymbol{R}_{\triangle}^{-1} \vec{B}_{\triangle 2}(\boldsymbol{R}_{\triangle} \vec{r}), \tag{3}$$

$$\boldsymbol{R}_{\triangle} = \begin{pmatrix} -1 & 0 & 0 \\ 0 & 1 & 0 \\ 0 & 0 & -1 \end{pmatrix}. \tag{4}$$

The matrix $\boldsymbol{R}_{\triangle}$ is a rotation matrix of 180° around the y-axis and can therefore be used to calculate field for both cases. On the other hand, direct implementation of the field expressions for both surfaces provides a faster algorithm.

For $z = 0$, the expression for B_z produces no valid result, as some of the terms are divided by zero. Research of the magnetic field [9] around this surface has shown that $\lim_{z \to 0} B_z = 0$. The expressions also do not solve correctly at the vertical side planes of the triangular shape, for $\triangle 1$ defined by $x = b, y = (b/a)x$ and $y = -b$. The authors were not able to analytically solve this problem, and have therefore implemented linear interpolation around those non-solving points. Such an approach works very good, as can be seen from the flux density graphs in Section IV.

TABLE II
ROTATION MATRIX AND REFERENCE POINT IN GLOBAL COORDINATES FOR EACH SURFACE OF THE PYRAMIDAL FRUSTUM

Surface	$\boldsymbol{R}_m$	${}^G\vec{O}_m$			
1	$\boldsymbol{I}$	$[\ 0$	0	$-c$	$]^T$
2	$\boldsymbol{I}$	$[\ 0$	0	c	$]^T$
3	$\boldsymbol{R}_1$	$[\ -a_{mid}$	$-b_{mid}$	0	$]^T$
4	$\boldsymbol{R}_1$	$[\ -a_{mid}$	0	0	$]^T$
5	$\boldsymbol{R}_1$	$[\ -a_{mid}$	b_{mid}	0	$]^T$
6	$\boldsymbol{R}_2$	$[\ -a_{mid}$	b_{mid}	0	$]^T$
7	$\boldsymbol{R}_2$	$[\ 0$	b_{mid}	0	$]^T$
8	$\boldsymbol{R}_2$	$[\ a_{mid}$	b_{mid}	0	$]^T$
9	$\boldsymbol{R}_3$	$[\ a_{mid}$	b_{mid}	0	$]^T$
10	$\boldsymbol{R}_3$	$[\ a_{mid}$	0	0	$]^T$
11	$\boldsymbol{R}_3$	$[\ a_{mid}$	$-b_{mid}$	0	$]^T$
12	$\boldsymbol{R}_4$	$[\ a_{mid}$	$-b_{mid}$	0	$]^T$
13	$\boldsymbol{R}_4$	$[\ 0$	$-b_{mid}$	0	$]^T$
14	$\boldsymbol{R}_4$	$[\ -a_{mid}$	$-b_{mid}$	0	$]^T$

C. Field of the Pyramidal Frustum

It was shown in Fig. 3 that fourteen rectangular and triangular surfaces are identified within the pyramidal frustum. With the field expressions for the rectangular surface and those for the triangular charged surface, the magnetic field of the pyramidal frustum is obtained. The charge density of each surface is defined by the inproduct

$$\sigma = \vec{M} \cdot \vec{\hat{n}} = \mu_0^{-1} \vec{B}_r \cdot \vec{\hat{n}}. \tag{5}$$

The vectors $\vec{M}$ and $\vec{B}_r$ are the magnetization and remanent flux density of the PM, respectively, and $\vec{\hat{n}}$ is the normal vector of the surface. By applying this equality to all surfaces, the condition that the net magnetic charge of the PM must be zero is satisfied.

At a random observation point in global coordinates ${}^L\vec{r}$ the magnetic field induced by surface m (with $m = 1 \ldots 14$) is obtained by

$${}^G\vec{B}_m(\vec{r}) = \boldsymbol{R}_m^{-1}\, {}^L\vec{B}_m(\boldsymbol{R}_m({}^G\vec{r} - {}^G\vec{O}_m)). \tag{6}$$

The vector $({}^G\vec{r} - {}^G\vec{O}_m)$ defines the relative position of the observation point ${}^G\vec{r}$ with respect to the reference point ${}^G\vec{O}_m$ of surface m in global coordinates. Table II defines these reference points. This table also indicates which rotation matrix $\boldsymbol{R}_{1\ldots4}$ must be applied for the respective surfaces. Multiplication with the rotation matrix $\boldsymbol{R}_{1\ldots4}$ transforms the global coordinates into the local coordinates of surface m, after which ${}^L\vec{B}_m$ is obtained. Finally, multiplication of ${}^L\vec{B}_m$ with the inverse rotation matrix $\boldsymbol{R}^T$ transforms the magnetic field expression from local to global coordinates, hence, gives ${}^G\vec{B}_m$.

The rotation matrices $\boldsymbol{R}_{1\ldots4}$ and the variables a_{mid} and b_{mid} from Table II are given by the equations below. The matrix $\boldsymbol{I}$ is the unity matrix.

$$\boldsymbol{R}_1 = \begin{pmatrix} 0 & -1 & 0 \\ \cos(\alpha_1) & 0 & \sin(\alpha_1) \\ -\sin(\alpha_1) & 0 & \cos(\alpha_1) \end{pmatrix}, \tag{7}$$

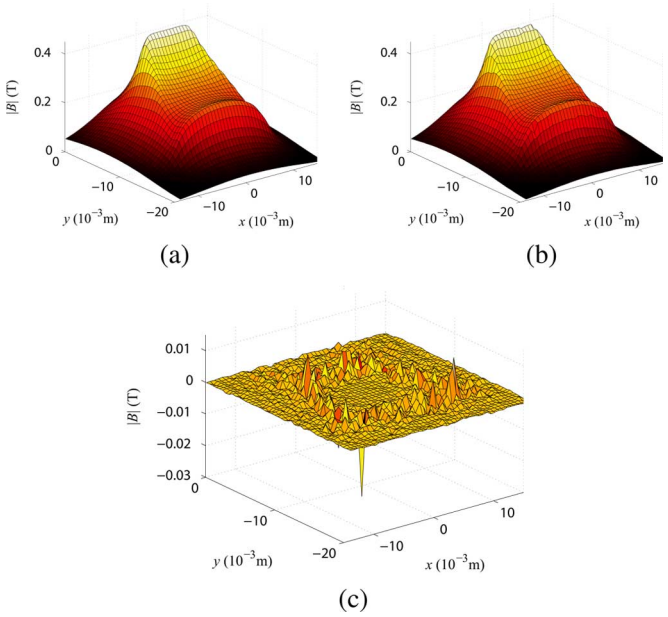

Fig. 5. Field calculation on a surface parallel to surface 10. Analytical results in (a), FEM results in (b) and their difference in (c).

$$\boldsymbol{R}_2 = \begin{pmatrix} -1 & 0 & 0 \\ 0 & -\cos(\alpha_2) & -\sin(\alpha_2) \\ 0 & -\sin(\alpha_2) & \cos(\alpha_2) \end{pmatrix}, \tag{8}$$

$$\boldsymbol{R}_3 = \begin{pmatrix} 0 & 1 & 0 \\ -\cos(\alpha_3) & 0 & -\sin(\alpha_3) \\ -\sin(\alpha_3) & 0 & \cos(\alpha_3) \end{pmatrix}, \tag{9}$$

$$\boldsymbol{R}_4 = \begin{pmatrix} 1 & 0 & 0 \\ 0 & \cos(\alpha_4) & \sin(\alpha_4) \\ 0 & -\sin(\alpha_4) & \cos(\alpha_4) \end{pmatrix}, \tag{10}$$

$$a_{\text{mid}} = \frac{a_t + a_b}{2}, \tag{11}$$

$$b_{\text{mid}} = \frac{b_t + b_b}{2}. \tag{12}$$

Vectorial summation of the magnetic fields obtained by (6) over the fourteen surfaces provides exact analytical expressions for the magnetic field, ${}^G\vec{B}$, of the pyramidal frustum.

IV. FIELD AND FORCE VERIFICATION

A finite element modeling (FEM) software package [11] is used to verify the analytical field expressions of the interaction field. Dimensions are those of PM1 shown in Table III. Figs. 5(a) and (b) show the magnetic flux density, $|\vec{B}|$, obtained analytically and the flux density obtained by means of FEM, respectively. The tested surface is parallel to and 1 mm separated from surface 10 (Fig. 3). The difference between analytical and FEM results (Fig. 5(c)) is very low (with an absolute mean value is $7.3 \cdot 10^{-4}$T). Comparison with the FEM results in Fig. 5(b) which clearly are noisy, reveals that this error is mainly due to numerical noise in FEM.

Although that the calculation time is very low, the analytical expressions of the magnetic field induced by a pyramidal-

TABLE III
DIMENSIONS AND ORIENTATION OF THE PYRAMIDAL FRUSTA USED FOR VERIFICATION

PM1	a_{bot}	10	mm	a_{top}	5	mm
	b_{bot}	15	mm	b_{top}	5	mm
	c	5	mm	B_r	$1.23\ {}^1\vec{e}_z$	T
	${}^G\vec{O}_1$	$\begin{bmatrix}0\\0\\0\end{bmatrix}$	mm	$\boldsymbol{R}$	$\begin{bmatrix}1&0&0\\0&1&0\\0&0&1\end{bmatrix}$	
PM2	a_{bot}	10	mm	a_{top}	5	mm
	b_{bot}	15	mm	b_{top}	5	mm
	c	5	mm	B_r	$1.23\ {}^2\vec{e}_z$	T
	${}^G\vec{O}_2$	$\begin{bmatrix}5\\0\\15\end{bmatrix}$	mm	$\boldsymbol{R}$	$\begin{bmatrix}-1&0&0\\0&1&0\\0&0&-1\end{bmatrix}$	

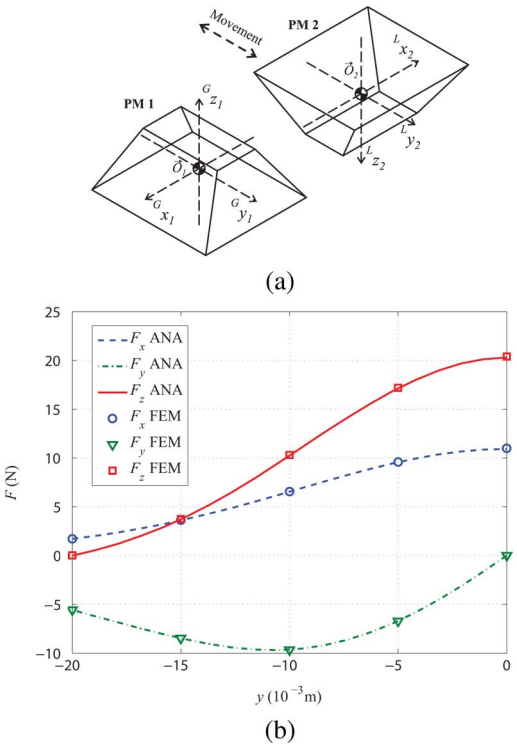

Fig. 6. Semi-analytical (dashed) and FEM results obtained for the interaction force between the PMs.

frustum shaped PM are rather complicated [9]. This makes integration of these fields over a surface, necessary for analytical force calculation, very difficult to achieve. Therefore, the Maxwell Stress Tensor (MST) method [10] is used in this paper to obtain the interaction force. Although being semi-analytical, it provides very accurate calculation of the interaction force between PMs. This is illustrated in Fig. 6, which shows the simulation results obtained by MST (0.5 mm discretization), and FEM for two pyramidal frusta which are moved with respect to each other. Dimensions and orientation of both PMs are shown in Table III. The figure demonstrates that the MST method is a highly accurate method for modeling the interaction force between pyramidal-frustum shaped PMs and is therefore very suitable to be used in the design process of a PM based gravity compensator.

V. CONCLUSION

This paper presents a novel method to obtain fully analytical expressions of the magnetic field created by a pyramidal-frustum shaped permanent magnet. Fourteen rectangular and triangular surfaces are identified which form the pyramidal frustum. A method to derive the analytical field expressions for the triangular shaped charged surface is presented, together with a short discussion on validity of the mathematical solution. Matrix translations and rotations are subsequently used to obtain the analytical field expressions for the pyramidal frustum. These expressions are validated using FEM results. Using the Maxwell Stress Tensor method the force is obtained semi-analytically. Results match closely with FEM results. This method allows a relatively fast calculation of the field and interaction force of arrays with pyramidal-shaped PMs.

REFERENCES

[1] K. Choi, Y. Cho, T. Shinshi, and A. Shimokohbe, "Stabilization of one degree-of-freedom control type levitation table with permanent magnet repulsive forces," *Mechatron.*, vol. 13, pp. 587–603, 2002.
[2] W. Robertson, B. Cazzolato, and A. Zander, "A multipole array magnetic spring," *IEEE Trans. Magn.*, vol. 41, no. 10, pp. 3826–3828, Oct. 2005.
[3] J. Janssen, J. Paulides, and E. Lomonova, "Passive magnetic suspension limitations for gravity compensation," *J. Syst. Design Dyn.*, vol. 3, no. 3, 2009, to be published.
[4] M. Lee and D. Gweon, "Optimal design of a double-sided linear motor with a multi-segmented trapezoidal magnet array for a high precision positioning system," *J. Magn. Magn. Mater.*, vol. 281, pp. 336–346, Jun. 2004.
[5] K. Meessen, B. Gysen, J. Paulides, and E. Lomonova, "Halbach permanent magnet shape selection for slotless tubular actuators," *IEEE Trans. Magn.*, vol. 44, no. 11, pp. 4305–4308, Nov. 2008.
[6] C. Xia, H. Li, and T. Shi, "3-D magnetic field and torque analysis of a novel Halbach array permanent-magnet spherical motor," *IEEE Trans. Magn.*, vol. 44, no. 8, pp. 2016–2020, Aug. 2008.
[7] G. Akound and J.-P. Yonnet, "3-D analytical calculation of the forces exerted between two cuboidal magnets," *IEEE Trans. Magn.*, vol. MAG-20, no. 5, pp. 1962–1964, Sep. 1984.
[8] F. Bancel, "Magnetic nodes," *J. Appl. Phys.*, vol. 32, pp. 2155–2161, Jun. 1999.
[9] J. Janssen, J. Paulides, and E. Lomonova, "Skewed linear permanent magnet actuator: 3D analytical field calculation using triangular magnet segments," *Compel*, 2009, to be published.
[10] E. Furlani, *Permanent Magnet and Electromechanical Devices: Materials, Analysis and Applications*, 6th ed. London, U.K.: Academic, 2001.
[11] *"Flux 10 User's Guide,"* 10.2.1 ed. 2008.